

Stepwise Unwinding of Polyelectrolytes under Stretching

M. N. Tamashiro*[†] and H. Schiessel[‡]

Materials Research Laboratory, University of California, Santa Barbara, California 93106-5130, and Department of Physics and Department of Chemistry and Biochemistry, University of California, Los Angeles, California 90095

Received December 3, 1999; Revised Manuscript Received April 17, 2000

ABSTRACT: We consider the unwinding of a tethered, flexible, and weakly charged polyelectrolyte in a salt-free poor solvent under an externally imposed strain. Using scaling arguments, we predict that the restoring force of a stretched polyelectrolyte shows a sawtooth pattern as a function of the externally imposed end-to-end distance. This nonmonotonic behavior arises from a cascade of conformational transitions between necklace-like structures with different number of beads. The transitions result from the interplay between the unscreened Coulomb repulsion of charged monomers and the short-range attraction of the backbone.

1. Introduction

Various water-soluble polymers, including essential biopolymers such as DNA and proteins, carry ionizable groups, which dissociate upon contact with a polar solvent. The solubility of these charged polymers—called polyelectrolytes (PE)—is significantly enhanced by the presence of the charged groups. The electrostatic repulsion between the charged monomers improves the PE solubility in solvents that would be poor for the uncharged backbone, providing a stabilizing mechanism against collapse and eventual precipitation. From the theoretical point of view, the challenge represented by the long-range Coulomb interaction makes the analytical description of PE more difficult than that of their neutral counterparts. (For a review on scaling approaches to PE, cf. ref 1 and references therein.)

Especially, the widespread case of a PE in a poor solvent shows an intricate behavior resulting from the competition between electrostatic repulsion and surface tension. The shape that minimizes the free energy of such a chain is usually the necklace configuration, which consists of compact charged globules connected via thin strings (see Figure 1). Such a conformation was first proposed by Kantor and Kardar² for polyampholytes (polymers with positively and negatively charged monomers) and was then extended to uniformly charged PE in poor solvent by Dobrynin, Rubinstein, and Obukhov.³ Besides the first analytical study by Dobrynin et al.,³ based on scaling arguments, this scenario is also supported by a variational approach⁴ as well as Monte Carlo³ and molecular dynamics simulations⁵ of dilute solutions of weakly charged PE. Small-angle neutron and small-angle X-ray scattering experiments performed with polystyrenesulfonate in water⁶ are at least consistent with the picture of necklace structures in semidilute solutions,⁷ although they do not represent a direct proof. We note that for a finite concentration of counterions (always present for a finite concentration of chains) a part of the counterions condense on sufficiently highly charged chains. This may lead to a chain collapse as demonstrated in a molecular dynamics

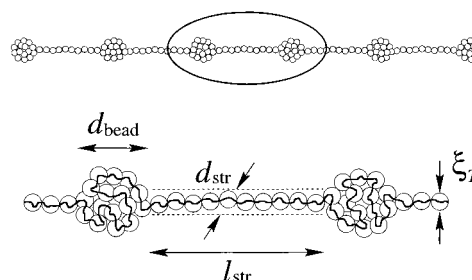


Figure 1. Necklace configuration composed of N_{bead} spherical beads with diameter d_{bead} joined by $(N_{\text{bead}} - 1)$ cylindrical strings ($N_{\text{bead}} = 6$ in the figure) with length l_{str} and diameter d_{str} . Each bead (string) contains m_{bead} (m_{str}) monomers, respectively. The monomer density of the beads and the strings is the same and follows from the densely packed thermal blobs of size ξ_T , i.e., $\rho = 6\tau/\pi b^3$.

simulation for multivalent counterions,⁸ consistent with scaling theories.^{7,9–11} Necklace configurations are, however, observed in molecular dynamics simulations of highly charged PE with partially condensed monovalent counterions.^{12,13} It still remains an open question whether and under which circumstances thermodynamically stable necklaces with condensed counterions really exist.

Besides recent theoretical progress in the understanding of charged polymers, there are also new experimental methods on-hand that allow the manipulation of individual macromolecules.¹⁴ Force measurement apparatus, including the atomic force microscope (AFM) and optical tweezers, allow to observe the stretching of single polymer chains. Experiments were performed on a variety of systems, including DNA,^{15–18} single chromatin fibers,¹⁹ the polysaccharide dextran,²⁰ and the protein titin.^{21–25} In particular, in the case of the giant protein titin, responsible for the elasticity of muscles, the force–extension profile obtained under stretching exhibits a prominent sawtooth pattern,^{24,25} which is attributed to the successive unfolding of immunoglobulin domains. This effect may be well explained as stepwise increases in the contour length of a polymer whose elastic properties are described by the wormlike chain model (WLC). In fact, Monte Carlo simulations combining WLC elasticity with a thermodynamical two-state model²⁶ reproduce the experimental data very well. A similar two-state model has also been proposed

[†] University of California, Santa Barbara.

[‡] University of California, Los Angeles.

* Corresponding author. e-mail: mtamash@mrl.ucsb.edu.

to explain the stress-induced transformation of DNA between the B and S forms.²⁷ Both treatments focus on the elastic properties of the chain and do not discuss the role of the Coulomb interactions in the stress-driven transitions.

Motivated by these experiments, we perform a scaling analysis of the stretching of a weakly charged PE under poor solvent conditions, i.e., of a necklace. The process of unwinding such a structure may be of some importance for the denaturation of biopolymers under deformation or mechanical stress as well as for the stretching of synthetic PE. It is known that globular uncharged polymers subject to external forces undergo an abrupt (first-order) coil–stretched transition.^{28,29} Similar effects might be expected in the case of a necklace structure. Because most biopolymers, particularly DNA and proteins, are in fact electrically charged, it is important to investigate how the Coulomb repulsion affects their conformation and response to mechanical stress and strain (cf., e.g., ref 30). In fact, we will demonstrate in this paper that the necklace undergoes a stepwise unfolding under an externally imposed strain—similar to the behavior observed for titin mentioned above. Thus, a PE in a poor solvent represents a simple nonmicroscopic system to study this phenomenon.

The paper is organized as follows: In section 2 we review and refine the scaling arguments that lead to the necklace configuration for weakly charged PE under poor solvent conditions. In section 3 we obtain the steady-state configuration and the static restoring force of a stretched PE when the end-to-end distance is externally imposed. In section 4 we consider the effect of friction forces when a tethered PE is stretched from the rest at constant drift velocity. We conclude in section 5 with a discussion of the relevant mechanisms that lead to stepwise unfolding and give further examples of polymeric systems that may exhibit similar features. In Appendix A we obtain the contributions to the free energy of the necklace structure. In Appendix B we give the free energy of the tadpole configuration. In Appendix C we show the validity of the quasi-static steady-state approximation.

2. Scaling Theory for Weakly Charged PE

We consider a dilute solution of flexible PE under poor solvent conditions at a temperature ΔT below the Θ temperature. This is the temperature at which the second virial coefficient between polymer segments vanishes so that the conformation of each chain corresponds to that of an ideal random walk. The chains contain $N \gg 1$ monomers of size b , and a fraction ϕ of the monomers are charged. To avoid the phenomenon of counterion condensation, which decreases the effective charge of the PE and may change its conformational properties,^{10,11} we restrict our analysis to the case of weakly charged PE ($u^2\phi \ll 1$), where $u = l_B/b$ is the ratio of the Bjerrum length $l_B = e^2/\epsilon k_B T$ to the monomer size b (e is the electronic charge, ϵ is the dielectric constant of the solvent, k_B is the Boltzmann constant, and T is the temperature). Highly charged PE and the effect of counterion condensation, which may lead to an instability of the necklace structure, will be discussed in a forthcoming paper.³¹ Furthermore, we will assume a salt-free environment, so that there is no screening of the Coulomb repulsion between the charged monomers due to excess ions.

For uncharged polymers ($u^2\phi = 0$) and close to the Θ temperature ($\tau N^{1/2} < 1$), where $\tau = \Delta T/\Theta$ denotes the

relative deviation from the Θ temperature (a measure for the solvent quality), the chain behaves like an ideal Gaussian coil³² of size

$$R \sim N^{1/2} b \quad (1)$$

where the symbol \sim is used to state a scaling relation, which ignores numerical prefactors. On the other hand, under poor solvent conditions occurring for temperatures sufficiently below the Θ point or sufficiently large chains ($\tau N^{1/2} > 1$), the short-range attraction between monomers of the backbone results in a collapse of the chain into a spherical globule^{32,33} of radius

$$R \sim (N/\tau)^{1/3} b \quad (2)$$

and density

$$\rho \sim \tau/b^3 \quad (3)$$

On length scales smaller than the size of the thermal density fluctuations, $\xi_T = b/\tau$, the attractive interactions can be neglected, and the chain obeys Gaussian statistics. On length scales larger than ξ_T the collapsed chain may be pictured as composed of close-packed thermal blobs of size ξ_T containing $g_T = (\xi_T/b)^2 = 1/\tau^2$ monomers.

For weakly charged PE ($u^2\phi \ll 1$) and close to the Θ temperature ($\tau N^{1/2} < 1$), the length scale below which the chain preserves its ideal shape, remaining unperturbed by the Coulomb repulsion, is the electrostatic blob size,³⁴ $\xi_{el} = b(u\phi^2)^{-1/3}$. On length scales larger than ξ_{el} , the electrostatic repulsion dominates and extends the chain into a linear array of electrostatic blobs of size ξ_{el} containing $g_{el} = (\xi_{el}/b)^2 = (u\phi^2)^{-2/3}$ monomers. In close analogy to the Pincus blob picture for a stretched chain under external forces,³⁵ the chain assumes a rodlike shape of length

$$L \sim \frac{N}{g_{el}} \xi_{el} = Nb(u\phi^2)^{1/3} \quad (4)$$

For weakly charged PE ($u^2\phi \ll 1$) under poor solvent conditions ($\tau N^{1/2} > 1$), the conformation of the chain is governed by the competition between the long-range Coulomb repulsion of charged monomers and the surface tension originated from the short-range attraction of the backbone (poor solvent condition). Khokhlov⁹ suggested that, to optimize its free energy, the collapsed chain deforms into an elongated cylindrical globule of length

$$L_{cyl} \sim Nb(u\phi^2)^{2/3}/\tau \quad (5)$$

and thickness

$$D \sim b(u\phi^2)^{-1/3} = \xi_{el} \quad (6)$$

However, the cylindrical geometry is locally unstable, analogous to the classical problem of a charged liquid droplet, considered by Lord Rayleigh³⁶ more than one century ago. He predicted that a charged liquid droplet, above a certain critical charge, spontaneously deforms and splits into smaller droplets separated by an infinite distance, each droplet carrying a lower charge than the critical one. Because of the covalent bonds of the backbone, it is not allowed for the monomers to dissociate, and this equilibrium state is unreachable for a PE chain. However, the system can reduce its energy by

rearranging into a set of smaller compact charged globules (beads) connected by narrow strings—the necklace configuration.³

Consider now the necklace configuration with N_{bead} spherical beads of size d_{bead} joined by $(N_{\text{bead}} - 1)$ cylindrical strings of length l_{str} and width d_{str} , depicted in Figure 1. The total length of the necklace is given by

$$L = N_{\text{bead}}d_{\text{bead}} + (N_{\text{bead}} - 1)l_{\text{str}}, \quad N_{\text{bead}} \geq 2 \quad (7)$$

The number of monomers per bead is denoted by m_{bead} and the number of monomers per string by m_{str} . Since the electrostatic repulsion between charged monomers does not affect significantly the volume occupied by the PE, we assume that the beads as well as the strings are still composed of close-packed thermal blobs, i.e.

$$d_{\text{bead}} = b \left(\frac{m_{\text{bead}}}{\tau} \right)^{1/3} \quad (8)$$

$$l_{\text{str}} = \frac{2b^3 m_{\text{str}}}{3\tau d_{\text{str}}^2} \quad (9)$$

resulting in a monomer density $\rho = 6\tau/\pi b^3$. (One has $g_T = 1/\tau^2$ monomers per spherical thermal blob of radius $b/2\tau$.) Introducing the total number of monomers inside all the strings,

$$M_{\text{str}} = N - N_{\text{bead}}m_{\text{bead}} \quad (10)$$

we are led to

$$m_{\text{bead}} = \frac{N - M_{\text{str}}}{N_{\text{bead}}} \quad (11)$$

$$m_{\text{str}} = \frac{M_{\text{str}}}{N_{\text{bead}} - 1} \quad (12)$$

The total free energy of the necklace configuration may be split into five terms,

$$\mathcal{F} = \mathcal{F}_s + \mathcal{F}_b + \mathcal{F}_{\text{bb}} + \mathcal{F}_{\text{bs}} + \mathcal{F}_{\text{ss}} \quad (13)$$

where the different terms account for intra-string, intra-bead, inter-bead, inter-bead-string, and inter-string interactions, respectively. In contrast to previous simple scaling arguments,³ we perform here a more detailed calculation taking all numerical and geometrical prefactors into account. These refinements are required here because the energy barriers between the different necklace structures are smaller in the stretched states under investigation than in the unstretched case. We also mention that the optimum lowest energy necklace structure for a given number of beads *is not* comprised by identical subunits, but rather contains slightly polydisperse nonequidistant beads. This effect follows from the long-ranged nature of the Coulomb interaction and finite-size effects. A necklace composed of monodisperse beads would correspond to the optimal configuration only if the beads would not interact. Nevertheless, since the determination of the exact lowest energy polydisperse-bead structure is hardly feasible and leads only to minor deviations from the monodisperse-bead necklace, we assume in the following that all beads have the same size and are equally spaced.

The different contributions to the free energy of the necklace, eq 13, are rather complicated and are rel-

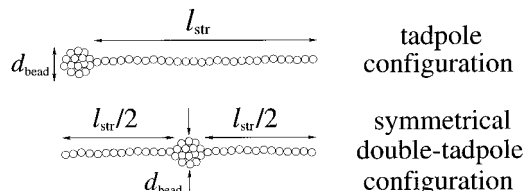


Figure 2. Two stretched conformations with $N_{\text{bead}} = 1$: the tadpole and the symmetrical double-tadpole configurations.

egated to Appendix A. The minimization of the total free energy, eq 13, with respect to N_{bead} , M_{str} , and d_{str} leads to the optimal values of the necklace configuration. In a previous calculation, Dobrynin et al.³ neglected all numerical prefactors, treated N_{bead} as a continuous variable, and made additionally two approximations. The total length of the necklace structure was obtained in the limit of a string much longer than a bead, $l_{\text{str}} \gg d_{\text{bead}}$,

$$L \approx (N_{\text{bead}} - 1)l_{\text{str}} = \frac{b^3}{\tau d_{\text{str}}^2} M_{\text{str}} \quad (14)$$

and the sum of the three inter-energy repulsion terms, given by eqs A.11–A.13, was approximated by

$$\frac{1}{k_B T} (\mathcal{F}_{\text{bb}} + \mathcal{F}_{\text{bs}} + \mathcal{F}_{\text{ss}}) \approx \frac{l_B \phi^2 N^2}{L} \quad (15)$$

With these approximations, Dobrynin et al. were able to show that, for a certain range of parameters,³ the equilibrium configuration of a weakly charged PE in the absence of external forces is a necklace structure with number of beads

$$N_{\text{bead}}^0 \approx N \tau^2 \left(\frac{\xi_T}{D} \right)^3 = \frac{Nu\phi^2}{\tau} \quad (16)$$

and length (at rest)

$$L_0 \approx Nb\tau \left(\frac{\xi_T}{D} \right)^{3/2} = Nb \left(\frac{u\phi^2}{\tau} \right)^{1/2} \quad (17)$$

As we will consider the transitions driven by the competition between the different terms by stretching the PE, it is important to keep all numerical prefactors. Especially, as mentioned earlier, the distinct necklace configurations with different number of beads have small free energy differences under external forces, because all structures converge to a stretched cylinder upon strong strain. Therefore, we will use the more refined approximations given by eqs A.11–A.13, which yield a repulsion energy that depends on the number of beads, instead of eq 15. Therefore, in our formulation the unstretched equilibrium configuration *is not given* by eqs 16 and 17, but rather follows from the numerical minimization of the total free energy (13).

Up to now we considered just necklace structures with $N_{\text{bead}} \geq 2$. However, by stretching a PE, we may also find structures with just one bead ($N_{\text{bead}} = 1$). Figure 2 sketches two of these configurations: a half-dumbbell (tadpole) and a symmetrical double-tadpole. In the tadpole configuration, we have just one single rod attached to a spherical globule. In the symmetrical double-tadpole configuration, we have two identical rods pointing in opposite directions, radially aligned with the center of the spherical globule. It turns out that the free

energy associated with all possible double-tadpole configurations is always higher than that associated with the tadpole configuration. This is due to the bead-string repulsion, which is smaller for the tadpole configuration. The free energy of the tadpole configuration is discussed in Appendix B. Although the tadpole configuration is energetically not favorable in the absence of applied forces, we will show in the next section that it occurs when a necklace chain becomes highly stretched.

Further stretching of the PE (after the unraveling of the last bead of the tadpole configuration) yields a highly stretched cylindrical globule, similar to that found under Θ conditions. In the same spirit of the approximations performed for the strings of the necklace structure (see Appendix A), we compute the free energy of the cylindrical configuration of length $L = \xi_T \hat{L}$,

$$\begin{aligned} \frac{F^{\text{cyl}}}{k_B T} &= \frac{6\hat{N}^2}{5\hat{D}^3\hat{L}} \omega\left[\left(\frac{3\hat{L}^3}{2\hat{N}}\right)^{1/2}\right] + \left(\frac{2}{3}\hat{N}\hat{L}\right)^{1/2}, \quad \text{for } \hat{L} < \hat{L}_{\text{cross}} \\ &= \frac{6\hat{N}^2}{5\hat{D}^3\hat{L}} \omega\left(\frac{3\hat{L}^2}{2\hat{N}}\right) + \frac{3\hat{L}^2}{2\hat{N}}, \quad \text{for } \hat{L} > \hat{L}_{\text{cross}} \end{aligned} \quad (18)$$

where $\hat{N} = N\tau^2$, $\omega(x) = \text{arccosh}(x)/\sqrt{1-x^2}$, and recalling that $D = \xi_T \hat{D}$ is the thickness of the Khokhlov *unstretched* cylindrical globule, eq 6. The crossover length $L_{\text{cross}} = \xi_T \hat{L}_{\text{cross}}$ with

$$\hat{L}_{\text{cross}} = \frac{2}{3}\hat{N} \quad (19)$$

is the length at which the thickness of the *stretched* cylinder becomes of the thermal blob size ξ_T . At PE lengths $L < L_{\text{cross}}$ the free energy of the cylinder has a surface tension contribution, whereas for $L > L_{\text{cross}}$ the main contribution of the free energy comes from the entropic stretching of a Gaussian coil. At this length the free energy of the cylindrical and the tadpole configurations should be the same, although we observe a very small difference due to the approximations performed. In fact, the free energies of all necklace structures should also reduce to the cylinder value at the crossover length. Despite the approximations, we are able to obtain this convergence within fractions of $k_B T$. We observe that, for $L < L_{\text{cross}}$, the cylindrical configuration has always a higher free energy than that of the necklace/tadpole. Only after the last bead is unfolded, which occurs around the crossover length L_{cross} , we expect that the lowest energy configuration of the PE is a Θ solventlike cylinder with thickness smaller than the thermal blob size ξ_T .

3. Steady-State Configuration of a Stretched PE with Externally Imposed End-to-End Distance

A typical experimental setup in which a single macromolecule is stretched by an AFM tip^{20,24} is depicted in Figure 3. In our PE model picture, we start from a necklace configuration at rest with an initial number of beads N_{bead}^0 and natural length L_0 , both determined by the minimization of the total free energy (13). The polymer chain is adsorbed at one end to a flat (gold or mica) surface, and the other end is bounded to an AFM tip. The flat surface is moved away from the AFM tip (see Figure 3), imposing an external strain $L > L_0$ on the chain. We assumed that the PE chain is

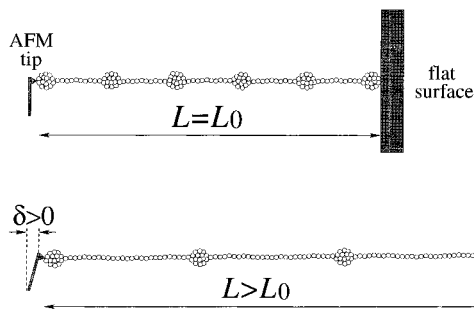


Figure 3. Our PE model system corresponding to the experimental setup in which a single PE chain is stretched by an AFM tip. The adsorbed chain, immersed in a salt-free poor solvent, takes at rest a necklace-like conformation. The chain is attached to an AFM tip and stretched by moving the flat surface away from the tip. In most cases the number of beads decreases as the PE is stretched. The force exerted on the polymer as a function of the end-to-end distance L is measured by a small deflection δ of the cantilever spring.

chemically adsorbed onto a neutrally charged flat surface and that image-charge effects due to the solvent/surface dielectric contrast are negligible. In the case of physical adsorption, when the chain is electrostatically bound to the oppositely charged surface, the detachment of single PE chains leads to a plateau in the force-extension profile.^{37,38}

Instead of using the approximated linear relation 14 for M_{str} as a function of L , we evaluate it by taking the real positive solution of the cubic equation

$$\hat{L} = \frac{L}{\xi_T} = N_{\text{bead}}^{2/3}(\hat{N} - \hat{M}_{\text{str}})^{1/3} + \frac{2}{3\hat{d}_{\text{str}}^2} \hat{M}_{\text{str}} \quad (20)$$

where $\hat{M}_{\text{str}} = M_{\text{str}}\tau^2$. For a fixed set of parameters (τ , u , ϕ , N) and an externally imposed end-to-end distance L , we minimize the total free energy with respect to \hat{d}_{str} for all possible structures (necklaces with $N_{\text{bead}} \geq 2$, the tadpole, and the cylindrical configurations), choosing the conformation with the lowest total free energy. For the range of parameters that we have explored, it turns out that the total free energy is minimized when the string thickness d_{str} assumes the thermal blob size ξ_T , which corresponds to $\hat{d}_{\text{str}} = 1$. The free energy minimization procedure allows us to construct the phase diagrams shown in Figures 4 and 5. The phase diagrams show the different states (characterized by the number of beads) in two cuts through the parameter space, one in the $\phi \times L$ plane and the other in the $\tau \times L$ plane (see figure captions for details). It can be seen that, by imposing a strain on the necklace, one induces transitions between states with different number of beads. Usually, the number of beads decreases with increasing end-to-end distance. Note, however, that in many cases there is an initial increase in the number of beads upon stretching, which occurs due to the reentrant behavior of the transition boundaries near the unstretched equilibrium length. Although at first sight unexpected, this reentrant behavior is required to match the Dobrynin et al. unstretched equilibrium results³ and the highly stretched cylinder at strong strain. Therefore, the conformational transitions of the PE under stretching are closely related to Dobrynin's force-free abrupt transitions upon variation of ϕ and/or τ .

In Figures 6 and 7 we present some geometrical properties of the necklace structure upon unraveling. In particular, Figure 7 shows that the total number of

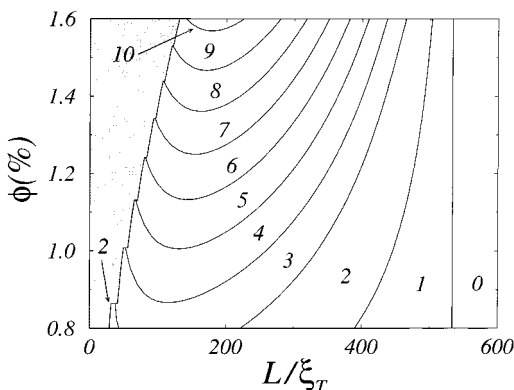


Figure 4. Diagram of states in the $\phi \times L$ space for $N = 5000$, $u = 2$, and $\tau = 0.4$. The number of beads labels distinct necklace configurations. “1” corresponds to the tadpole configuration, and “0” is a stretched cylinder with thickness smaller than the thermal blob size ξ_T . The gray region corresponds to compressed states, which were not treated in this work. The rightmost boundary of the gray region corresponds to the equilibrium lengths L_0 in the absence of external forces. In this case, we can clearly see the discontinuous nature of the transitions related to the jumps of the unstretched end-to-end distance L_0 , which become weaker as we increase the fraction ϕ of charged monomers. Note that for many values of ϕ one has first an initial increase in the number of beads upon stretching due to the reentrant behavior of the transition boundaries near the unstretched equilibrium line.

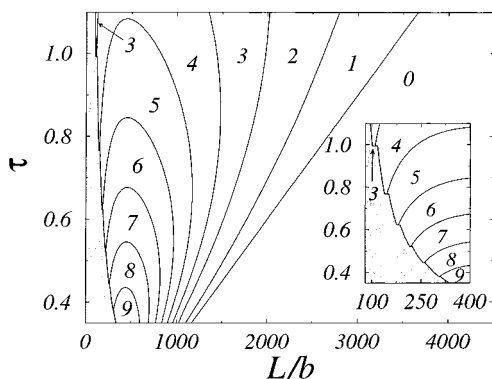


Figure 5. Diagram of states in the $\tau \times L$ space for $N = 5000$, $u = 2$, and $\phi = 1.5\%$. The interpretation of the numbers and the gray region are the same as in Figure 4. The inset presents a magnification of the region near the unstretched equilibrium line, showing the discontinuous nature of the transitions in the absence of external forces. Contrary to the previous example of constant τ and increasing ϕ , in this case the discontinuous jump of the unstretched end-to-end length L_0 becomes weaker as we decrease τ . For many values of τ there is also an initial increase in the number of beads upon stretching due to the reentrant behavior of the transition boundaries near the unstretched equilibrium line.

monomers in all strings M_{str} has only small jumps during the transitions. This means that the monomers of the unfolded bead essentially redistribute between the remaining beads. The transitions take place whenever—after sufficient stretching—the beads are so small that one of the beads can redistribute its monomers between the remaining beads without violating the Rayleigh criterion (corresponding to an upper bound for the bead size d_{bead}). For the first transition, however, due to the steep increase of the restoring force in the vicinity of the unstretched length, the critical upper bound for the bead size decreases faster than the (shrinking) size of the beads. Therefore, even though the size of the beads decreases, there is a Rayleigh instability that gives origin to the reentrant behavior

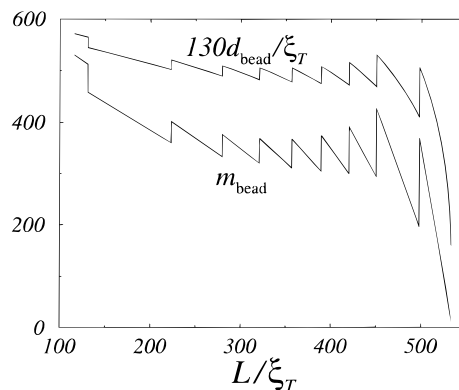


Figure 6. Number of monomers inside each bead m_{bead} and size of each bead d_{bead} , for the same set of parameters shown in Figure 9: $N = 5000$, $u = 2$, $\tau = 0.4$, and $\phi = 1.5\%$.

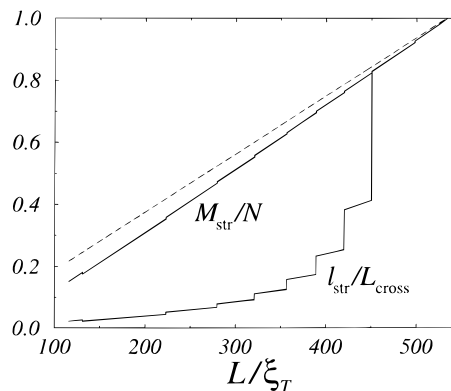


Figure 7. Total number of monomers in all strings M_{str} and length of each string l_{str} normalized to their final values, for the same set of parameters shown in Figure 9: $N = 5000$, $u = 2$, $\tau = 0.4$, and $\phi = 1.5\%$. For the two last stages of the unraveling, the dumbbell ($N_{\text{bead}} = 2$) and the tadpole ($N_{\text{bead}} = 1$) configurations, the two normalized curves are given by the same expression. The dashed curve represents the linear approximation 14 for M_{str} as a function of L (taking the numerical prefactor $2/3$ into account). Although this approximation describes well the behavior for high stretching, the deviation increases for smaller strains.

described in the last paragraph and the initial increase in the number of the beads.

To keep the PE chain at the externally imposed end-to-end distance $L > L_0$, one needs to apply an external force $F(L)$. In the experimental setup, this force may be measured by a small deflection δ of the AFM tip (see Figure 3). In the case of a static, time-independent, steady-state configuration, the external force $F(L)$ counterbalances simply the restoring force $-f(L)$,

$$F(L) = -f(L) = \frac{\partial \mathcal{F}}{\partial L} \quad (21)$$

Therefore, once we have obtained the lowest energy conformation, the restoring force may be evaluated by differentiation of the total free energy with respect to the end-to-end imposed length L . Typical static extension–force profiles are presented in Figures 8 and 9. They show a prominent sawtooth pattern, associated with the abrupt transitions between necklace configurations with a different number of beads. Despite the differences in the mechanism of unfolding, the stepwise behavior of the force–extension profile resembles the same effect observed in titin.^{24,25} For the set of parameters used in Figures 8 and 9, the necklace structures

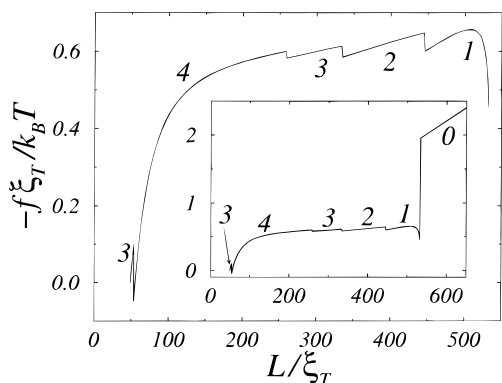


Figure 8. Static restoring force $-f$ as a function of the externally imposed end-to-end distance L for the set of parameters: $N = 5000$, $u = 2$, $\tau = 0.4$, and $\phi = 1\%$. For these parameters, the natural length L_0 of the PE is $L_0 = 48.9\xi_T$, and the necklace structure contains initially three beads ($N_{\text{bead}}^0 = 3$). Using the Bjerrum length of the water at room temperature, $l_B = 7 \text{ \AA}$, the normalizing factors are $k_B T \xi_T = 4.73 \text{ pN}$ and $\xi_T = 8.75 \text{ \AA}$. The number of beads labels the distinct necklace structures. Note the initial increase in the number of beads, which leads to a narrow negative-force window. The unwinding of the last bead occurs through a tadpole configuration (a spherical globule terminated by a cylindrical rod), labeled by "1". After the bead size d_{bead} reaches the string size d_{str} , which turns out to be of the thermal blob size ξ_T , the conformation of the PE is a highly stretched cylinder with thickness smaller than ξ_T , labeled by "0". As shown in the inset, for this highly stretched regime we expect that the force–extension relation is governed by the Pincus blob picture, $|f| \propto L$.

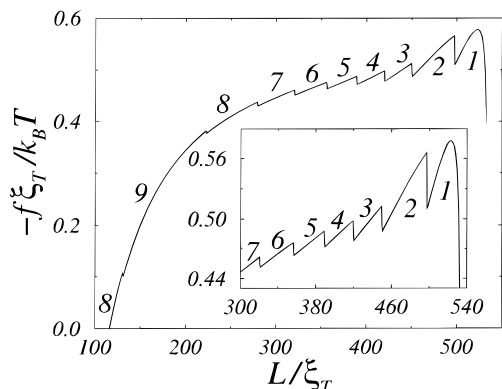


Figure 9. Static restoring force $-f$ as a function of the externally imposed end-to-end distance L for the set of parameters: $N = 5000$, $u = 2$, $\tau = 0.4$, and $\phi = 1.5\%$. For these parameters, the natural length L_0 of the PE is $L_0 = 116.2\xi_T$, and the necklace structure contains initially eight beads ($N_{\text{bead}}^0 = 8$). Using the Bjerrum length of the water at room temperature, $l_B = 7 \text{ \AA}$, the normalizing factors are $k_B T \xi_T = 4.73 \text{ pN}$ and $\xi_T = 8.75 \text{ \AA}$. Here we also have an initial increase in the number of beads. Analogous as shown in Figure 8, the strong-stress regime corresponding to a highly stretched cylinder with thickness smaller than ξ_T is governed by the Pincus linear relation, not presented here. To allow a better appreciation of the force–extension sawtooth pattern, the inset shows a magnification of the end portion of the curve.

at their equilibrium lengths in the absence of external forces contain initially three ($N_{\text{bead}}^0 = 3$) and eight ($N_{\text{bead}}^0 = 8$) beads, respectively. After an initial increase in the number of beads, they are successively unfolded as we increase the length of the PE.

We also give here the restoring force associated with the highly stretched state that follows from eq 18 with $L > L_{\text{cross}}$,

$$-\frac{f\xi_T}{k_B T} = \frac{1}{k_B T} \frac{\partial F^{\text{cy}}}{\partial L} = -\frac{6\hat{N}^2}{5\hat{D}^3\hat{L}^2} \omega\left(\frac{3\hat{L}^2}{2\hat{N}}\right) + \frac{18\hat{N}}{5\hat{D}^3} \omega'\left(\frac{3\hat{L}^2}{2\hat{N}}\right) + \frac{3\hat{L}}{\hat{N}} \quad (22)$$

which corresponds to the Pincus blob picture³⁵ (if we neglect contributions from the electrostatic repulsion). The PE forms a linear array of blobs of size $\xi_P = k_B T / |f|$ containing $g_P = (k_B T / |f| b)^2$ monomers, leading to a linear relation between externally imposed end-to-end distance and force,

$$L \sim \frac{N}{g_P} \xi_P = \frac{N b^2}{k_B T} |f| \quad (23)$$

We close this section by noting that there is a fundamental difference between an experiment where the end-to-end distance L is externally imposed (strain ensemble) and a situation with a given external force F (stress ensemble).³⁹ In the latter case one will not find a sequence of stepwise unfolding processes as response to an increasing applied tension. Instead, the structure will unfold at once when a critical value of the tension is reached. This value can be estimated by comparing the energy gain by stretching the necklace with the price that one has to pay by increasing its surface. If the necklace is stretched by a length ξ_T (the thermal blob size), one gains $-F\xi_T$. At the same time, one thermal blob is transferred from a globule to a string, which leads to an increase $\sigma\xi_T^2 = k_B T$ in the surface energy, where σ is the surface tension. The critical tension is $F_c = k_B T / \xi_T$, i.e., the tension at which the size of the Pincus blobs $\xi_P = k_B T / F$ equals the size of a thermal blob ξ_T . For $F > F_c$ the chain can be described by a sequence of Pincus blobs of total length $L \sim N b^2 F / k_B T$.

4. Dynamical Force–Extension Profile for Constant Pulling Velocity

The static restoring force $-f$ presented in Figures 8 and 9 corresponds to an equilibrium steady-state configuration. In other words, in the previous section we assumed that the flat surface is kept fixed after one reaches the externally imposed end-to-end length $L > L_0$. Most measurements, however, use a dynamical method to measure the force, being performed at constant pulling velocity V ,^{24–26}

$$L(t) = L_0 + Vt \quad (24)$$

Besides the static restoring force $-f$, we need to add a friction contribution, $f_{\text{friction}}(t)$, proportional to the product of the diameter of the bead, d_{bead} , by its drift velocity V_i , $i = 1, \dots, N_{\text{bead}}(t)$,

$$f_{\text{friction}}(t) = -3\pi\eta \sum_{i=1}^{N_{\text{bead}}(t)} d_{\text{bead}}(t) V_i(t) = -\frac{3}{2}\pi\eta V N_{\text{bead}}(t) d_{\text{bead}}(t) \quad (25)$$

where η is the shear viscosity of the solvent. To obtain eq 25, we have assumed a quasi-static equilibrium for the PE chain. In this case, the velocities of the beads are given simply by

$$V_i(t) = \frac{(i-1)V}{N_{\text{bead}}(t) - 1} \quad (26)$$

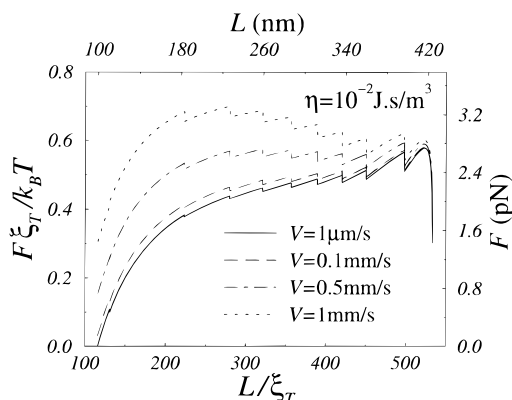


Figure 10. Measured force $F(t)$ as a function of the externally imposed end-to-end distance, $L = L_0 + Vt$, for the same set of parameters shown in Figure 9: $N = 5000$, $u = 2$, $\tau = 0.4$, and $\phi = 1.5\%$. The different curves show the effect of progressively faster pulling velocities, varying from $V = 1 \mu\text{m/s}$ to $V = 1 \text{mm/s}$. We used a shear viscosity $\eta = 10^{-2} \text{ J s/m}^3$. For the slowest drift velocity, the friction forces are too small, and the measured force is indistinguishable from the static restoring force presented in Figure 9. As we increase the pulling velocity, however, the friction contribution becomes more important.

Since the polymer has a constant drift velocity V , the sum of all forces on the PE must vanish, $F(t) + f + f_{\text{friction}}(t) = 0$. The measured force $F(t)$, given by

$$F(t) = -f - f_{\text{friction}}(t) = \frac{\partial \mathcal{F}}{\partial L} + \frac{3}{2} \pi \eta V N_{\text{bead}}(t) d_{\text{bead}}(t) \quad (27)$$

is plotted in Figure 10 for some pulling velocities V . Our treatment of the unraveling dynamics of a PE is based on the assumption of a quasi-static equilibrium of the necklace (see Appendix C), where the beads preserve their spherical geometry at each instant of time. Furthermore, we assume that there is a vanishing transient time for the beads to rearrange between the abrupt conformational transitions. Finite transient times yield a slower relaxation to the new conformation, broadening the troughs of the force–extension profile after the transitions. Despite the approximations, we see that some features resemble those experimentally observed in the unfolding of the titin:²⁴ (a) roughly equidistant peaks, (b) positive slope of the peaks (for small pulling velocities), and (c) increasing peak amplitude.

5. Discussion

In this paper we have shown that a PE in a poor solvent unfolds in a stepwise fashion under an externally imposed strain. The underlying mechanism is the successive unwinding of the beads of the necklace structure. As a result, the force–extension profile shows a characteristic sawtooth pattern. A similar profile is found in unfolding experiments on titin.²⁴ However, while in titin the sawtooth pattern is due to the unfolding of protein domains associated with specific interactions, here they arise from conformational transitions of an initially *structureless* PE. This suggests that, despite the diversity in the mechanisms of unfolding, the stepwise behavior of the force–extension profile may represent a rather general phenomenon.

What are the minimal requirements that lead to stepwise unfolding? And are there other systems that exhibit similar features? In fact, one should expect a wide variety of systems that show this behavior. Especially, polymer chains that self-assemble into a chain

of subunits connected by strings are promising candidates. Polyampholytes show a necklace structure with multidisperse beads.² Polysoaps (polymers where a fraction of the monomers is amphiphilic) self-assemble into a chain of micelles.⁴⁰ Polyelectrolytes that complex with oppositely charged macroions may form necklaces, where each “pearl” consists out of a macroion with a part of the PE chain wrapped around.⁴¹ The nucleosome filament of chromatin, a complex of DNA with oppositely charged histone octomers, is a famous example for this type of structure.⁴² We expect that all these systems unfold in a stepwise fashion. Important is here that the self-assembled subunits do not condense into one big homogeneous aggregate, like is the case for a neutral polymer in a poor solvent. In this particular example one expects just a plateau in the force–extension curve, which corresponds to the unraveling of the globule, but no sawtooth pattern.²⁸ Thus, one needs a mechanism that ensures an upper bound for the size of the subunits. The other important ingredient is a mechanism that leads to an increase in the free energy when the size of the subunit is decreased upon stretching. The interplay between these two competing mechanisms, which are not necessarily of the same origin, ensures an optimal size for the subunit. To make this more transparent, we give in Table 1 an overview over different polymeric systems and list the corresponding self-assembled subunits, the mechanisms that limit the size of these subunits, and the penalty one has to pay when one lowers their size as a result of chain stretching. For proteins, the unfolding depends on their detailed structure and associated specific interactions (cf., e.g., ref 43).

The discrete stepwise character of the unfolding is not appreciated by most of the treatments on these systems. For polysoaps, for instance, one focuses on the coexistence of free amphiphiles and amphiphiles in the micelles, which leads to a plateau in the force–extension profile.⁴⁰ Indeed, also our analysis shows roughly a plateau, but a closer inspection reveals the sawtooth pattern on top of it (cf. for instance Figure 8). Other investigations are devoted to the case of an externally applied constant force. This situation is much simpler: when the force reaches a certain threshold value, all subunits unfold simultaneously—at least, for identical subunits—associated with a jumpwise increase of the end-to-end distance. The resulting monotonic stress–strain characteristics was studied, for instance, for the case of a polyampholytic necklace in an external electric field (see ref 44 and references therein). We hope that micromechanical experiments will be able to test these predictions directly.

Note Added: After the submission of this work we became aware of the preprint by Vilgis et al.,⁴⁵ in which complementary topics of the same subject are considered.

Acknowledgment. We are grateful to P. Pincus for suggesting and discussing this problem and to A. W. C. Lau for bringing our attention to some relevant related work. M.N.T. acknowledges the financial support of the Brazilian agency CNPq—Conselho Nacional de Desenvolvimento Científico e Tecnológico. H.S. was supported by the National Science Foundation Grant DMR-97-08646. This research was also partially supported by the MRL Program of the National Science Foundation under Awards DMR-96-32716 and DMR-96-24091.

Table 1. Examples of Polymeric Systems That Self-Assemble into a String of Subunits; the Subunits Are Listed Together with the Mechanisms That Control Their Optimal Size

polymeric system	subunit that unfolds	limiting-size mechanism of subunits	penalty for lowering size of subunits
polyelectrolyte in poor solvent	spherical globule	Rayleigh instability	surface tension
polyampholyte	spherical globule (polydisperse)	Rayleigh instability (excess charge)	surface tension
polyelectrolyte–macroion complex	macroion plus wrapped chain	overcharging	undercharging
polysoap	micelle	headgroup interaction, coronal loops	surface tension
protein	folded domain	specific	specific

Appendix A. Free Energy of the Necklace Configuration

We give here a detailed discussion of the contributions to the total free energy of the necklace configuration, eq 13.

The intra-string free energy \mathcal{F}_s accounts for the electrostatic repulsion of charged monomers inside the strings plus their surface tension energy. If d_{str} decreases to a value smaller than ξ_T , we should replace the surface tension energy by the entropic energy of a stretched Gaussian coil. Hence

$$\frac{\mathcal{F}_s}{k_B T} = (N_{\text{bead}} - 1) \left[\frac{6I_B \phi^2 m_{\text{str}}^2}{5l_{\text{str}}} \omega(l_{\text{str}}/d_{\text{str}}) + \frac{l_{\text{str}} d_{\text{str}}}{\xi_T^2} \right], \quad \text{for } d_{\text{str}} > \xi_T$$

$$= (N_{\text{bead}} - 1) \frac{6I_B \phi^2 m_{\text{str}}^2}{5l_{\text{str}}} \omega(l_{\text{str}}/d_{\text{str}}) + \frac{3(N_{\text{bead}} - 1)^2 l_{\text{str}}^2}{2M_{\text{str}} b^2}, \quad \text{for } d_{\text{str}} < \xi_T \quad (\text{A.1})$$

with

$$\omega(x) = \frac{\text{arccosh}(x)}{(1 - x^{-2})^{1/2}} \quad (\text{A.2})$$

The geometrical prefactor for the string electrostatic energy was obtained by approximating it by a prolate ellipsoid of major semiaxis $a_> = l_{\text{str}}/2$ and two identical minor semiaxes $a_< = d_{\text{str}}/2$ carrying a charge $Q = e\phi m_{\text{str}}$, whose electrostatic self-energy is given by⁴⁶

$$U = \frac{3}{5} \frac{Q^2}{\epsilon a_>} \omega(a_>/a_<) \quad (\text{A.3})$$

The intra-bead free energy \mathcal{F}_b accounts for the electrostatic repulsion of charged monomers inside the beads plus their surface tension energy,

$$\frac{\mathcal{F}_b}{k_B T} = N_{\text{bead}} \left(\frac{6I_B \phi^2 m_{\text{bead}}^2}{5d_{\text{bead}}} + \frac{d_{\text{bead}}}{\xi_T^2} \right) \quad (\text{A.4})$$

The geometrical prefactor for the charged-sphere electrostatic self-energy was obtained using the limit $\lim_{x \rightarrow 1} \omega(x) = 1$.

The inter-bead free energy \mathcal{F}_{bb} takes the electrostatic repulsion between different beads into account,

$$\frac{\mathcal{F}_{\text{bb}}}{k_B T} = \frac{I_B \phi^2 m_{\text{bead}}^2}{2(l_{\text{str}} + d_{\text{bead}})} \sum_{i=1}^{N_{\text{bead}}} \sum_{j=1, j \neq i}^{N_{\text{bead}}} \frac{1}{|i-j|} = \frac{I_B \phi^2 m_{\text{bead}}^2}{l_{\text{str}} + d_{\text{bead}}} \sum_{k=1}^{N_{\text{bead}}-1} \left(\frac{N_{\text{bead}} - k}{k} \right)$$

$$= \frac{I_B \phi^2 m_{\text{bead}}^2}{l_{\text{str}} + d_{\text{bead}}} \{1 + N_{\text{bead}}[\gamma - 1 + \psi(N_{\text{bead}})]\} \quad (\text{A.5})$$

where $\gamma = 0.5772\dots$ is the Euler constant and ψ is the digamma function.⁴⁷ The above contribution corresponds to the energy of a linear arrangement of N_{bead} point charges $e\phi m_{\text{bead}}$ equidistant $l_{\text{str}} + d_{\text{bead}}$ apart.

The inter-bead–string free energy \mathcal{F}_{bs} follows from the electrostatic repulsion between beads and strings,

$$\frac{\mathcal{F}_{\text{bs}}}{k_B T} = \frac{8I_B \phi^2 m_{\text{str}} m_{\text{bead}}}{d_{\text{str}}^2 l_{\text{str}}} \sum_{i=0}^{N_{\text{bead}}-2} \sum_{j=0}^{N_{\text{bead}}-1} \int_0^{l_{\text{str}}} dz \times \int_0^{d_{\text{str}}/2} \frac{\rho d\rho}{\{\rho^2 + [z - (j - i)(l_{\text{str}} + d_{\text{bead}}) + d_{\text{bead}}/2]^2\}^{1/2}} \quad (\text{A.6})$$

The strings are assumed to be cylinders of length l_{str} and width d_{str} carrying a charge $e\phi m_{\text{str}}$.

Finally, the inter-string electrostatic repulsion \mathcal{F}_{ss} leads to

$$\frac{\mathcal{F}_{\text{ss}}}{k_B T} = \frac{8I_B \phi^2 m_{\text{str}}^2}{(\pi d_{\text{str}}^2 l_{\text{str}})^2} \sum_{i=0}^{N_{\text{bead}}-2} \sum_{j=0, j \neq i}^{N_{\text{bead}}-2} \int_0^{l_{\text{str}}} dz \int_0^{l_{\text{str}}} dz' \int_0^{d_{\text{str}}/2} \rho d\rho \int_0^{d_{\text{str}}/2} \rho' d\rho' \int_0^{2\pi} d\theta' \int_0^{2\pi} d\theta \frac{1}{\{\rho^2 + \rho'^2 - 2\rho\rho' \cos \theta + [z - z' - (j - i)(l_{\text{str}} + d_{\text{bead}})]^2\}^{1/2}}$$

$$= \frac{I_B \phi^2 m_{\text{str}}^2}{l_{\text{str}}^2} \sum_{k=1}^{N_{\text{bead}}-2} (N_{\text{bead}} - 1 - k) \times \left\{ \int_0^{l_{\text{str}}} dz \int_0^{l_{\text{str}}} \frac{dz'}{z - z' + k(l_{\text{str}} + d_{\text{bead}})} - \frac{d_{\text{str}}^2}{8} \int_0^{l_{\text{str}}} dz \int_0^{l_{\text{str}}} \frac{dz'}{[z - z' + k(l_{\text{str}} + d_{\text{bead}})]^3} \times \left[1 + \mathcal{O}\left(\frac{d_{\text{str}}^2}{l_{\text{str}}^2}\right) \right] \right\} \quad (\text{A.7})$$

The leading term corresponds to the interaction energy of charged *lines* with linear density $e\phi m_{\text{str}}/l_{\text{str}}$ aligned with the center of the beads and equally spaced d_{bead} apart along the longitudinal direction. Since the exact integral is awkward and this term leads only to minor contributions to the total free energy, we consider just the leading correction in d_{str} to the charged-line expression.

It is convenient to introduce scaled dimensionless variables,

$$\hat{N} = N\tau^2, \quad \hat{M}_{\text{str}} = M_{\text{str}}\tau^2, \quad \hat{d}_{\text{bead}} = \frac{d_{\text{bead}}}{\xi_T}, \quad \hat{\lambda}_{\text{str}} = \frac{l_{\text{str}}}{\xi_T},$$

$$\hat{d}_{\text{str}} = \frac{d_{\text{str}}}{\xi_T}, \quad \hat{D} = \frac{D}{\xi_T} \quad (\text{A.8})$$

in terms of which, after some algebraic manipulations, we may rewrite the contributions to the free energy,

$$\frac{\mathcal{F}_s}{k_B T} = \left[\frac{18\hat{d}_{\text{str}}^2}{10\hat{D}^3} \omega(\hat{l}_{\text{str}}/\hat{d}_{\text{str}}) + \frac{2}{3\hat{d}_{\text{str}}} \right] \hat{M}_{\text{str}}, \quad \text{for } \hat{d}_{\text{str}} > 1$$

$$= \left[\frac{18\hat{d}_{\text{str}}^2}{10\hat{D}^3} \omega(\hat{l}_{\text{str}}/\hat{d}_{\text{str}}) + \frac{2}{3\hat{d}_{\text{str}}^4} \right] \hat{M}_{\text{str}}, \quad \text{for } \hat{d}_{\text{str}} < 1 \quad (\text{A.9})$$

$$\frac{\mathcal{F}_b}{k_B T} = N_{\text{bead}} \left(\frac{6\hat{d}_{\text{bead}}^5}{5\hat{D}^3} + \hat{d}_{\text{bead}}^2 \right) \quad (\text{A.10})$$

$$\frac{\mathcal{F}_{\text{bb}}}{k_B T} = \frac{\hat{d}_{\text{bead}}^6}{\hat{D}^3(\hat{l}_{\text{str}} + \hat{d}_{\text{bead}})} \{1 + N_{\text{bead}}[\gamma - 1 + \psi(N_{\text{bead}})]\} \quad (\text{A.11})$$

$$\frac{\mathcal{F}_{\text{bs}}}{k_B T} = \frac{3\hat{d}_{\text{str}}^2 \hat{d}_{\text{bead}}^3}{\hat{D}^3} \sum_{k=1}^{N_{\text{bead}}-1} (N_{\text{bead}} - k) \left\{ \ln \left[\frac{\hat{z}_>(k)}{\hat{z}_<(k)} \right] + \ln \left[1 + \sqrt{1 + \left[\frac{\hat{d}_{\text{str}}}{2\hat{z}_>(k)} \right]^2} \right] - \ln \left[1 + \sqrt{1 + \left[\frac{\hat{d}_{\text{str}}}{2\hat{z}_<(k)} \right]^2} \right] + \left[\frac{2\hat{z}_>(k)}{\hat{d}_{\text{str}}} \right]^2 \left[\sqrt{1 + \left[\frac{\hat{d}_{\text{str}}}{2\hat{z}_>(k)} \right]^2} - 1 \right] - \left[\frac{2\hat{z}_<(k)}{\hat{d}_{\text{str}}} \right]^2 \left[\sqrt{1 + \left[\frac{\hat{d}_{\text{str}}}{2\hat{z}_<(k)} \right]^2} - 1 \right] \right\} \quad (\text{A.12})$$

$$\frac{\mathcal{F}_{\text{ss}}}{k_B T} = \frac{9\hat{d}_{\text{str}}^4}{4\hat{D}^3} \sum_{k=1}^{N_{\text{bead}}-2} (N_{\text{bead}} - 1 - k) \left[\hat{z}_+(k) \ln \hat{z}_+(k) + \hat{z}_-(k) \ln \hat{z}_-(k) - 2\hat{z}_0(k) \ln \hat{z}_0(k) - \frac{\hat{d}_{\text{str}}^2 \hat{\lambda}_{\text{str}}^2}{8\hat{z}_+(k) \hat{z}_0(k) \hat{z}_-(k)} \right] \quad (\text{A.13})$$

with

$$\hat{z}_>(k) = k\hat{\lambda}_{\text{str}} + \left(k - \frac{1}{2}\right)\hat{d}_{\text{bead}} \quad (\text{A.14})$$

$$\hat{z}_<(k) = (k-1)\hat{\lambda}_{\text{str}} + \left(k - \frac{1}{2}\right)\hat{d}_{\text{bead}} \quad (\text{A.15})$$

$$\hat{z}_\pm(k) = (k \pm 1)\hat{\lambda}_{\text{str}} + k\hat{d}_{\text{bead}} \quad (\text{A.16})$$

$$\hat{z}_0(k) = k(\hat{\lambda}_{\text{str}} + \hat{d}_{\text{bead}}) \quad (\text{A.17})$$

$$\hat{\lambda}_{\text{str}} = \frac{2}{3\hat{d}_{\text{str}}^2} \left(\frac{\hat{M}_{\text{str}}}{N_{\text{bead}} - 1} \right) \quad (\text{A.18})$$

$$\hat{d}_{\text{bead}} = \left(\frac{\hat{N} - \hat{M}_{\text{str}}}{N_{\text{bead}}} \right)^{1/3} \quad (\text{A.19})$$

Appendix B. Free Energy of the Tadpole Configuration

The total free energy of the tadpole configuration has three contributions,

$$\mathcal{F}^t = \mathcal{F}_s^t + \mathcal{F}_b^t + \mathcal{F}_{\text{bs}}^t \quad (\text{B.1})$$

accounting for intra-string, intra-bead, and bead-string interactions, respectively.

The intra-string contribution \mathcal{F}_s^t for the tadpole configuration is given by eq A.9, while the intra-bead free energy \mathcal{F}_b^t may be obtained by taking $N_{\text{bead}} = 1$ in eq A.10. Finally, the bead-string interaction reads

$$\frac{\mathcal{F}_{\text{bs}}^t}{k_B T} = \frac{3\hat{d}_{\text{str}}^2 \hat{d}_{\text{bead}}^3}{2\hat{D}^3} \left\{ \ln \left(\frac{2\hat{l}_{\text{str}} + \hat{d}_{\text{bead}}}{\hat{d}_{\text{bead}}} \right) + \ln \left[1 + \sqrt{1 + \left(\frac{\hat{d}_{\text{str}}}{\hat{d}_{\text{bead}}} \right)^2} \right] - \ln \left[1 + \sqrt{1 + \left(\frac{\hat{d}_{\text{str}}}{2\hat{l}_{\text{str}} + \hat{d}_{\text{bead}}} \right)^2} \right] + \left(\frac{2\hat{l}_{\text{str}} + \hat{d}_{\text{bead}}}{\hat{d}_{\text{str}}} \right)^2 \left[\sqrt{1 + \left(\frac{\hat{d}_{\text{str}}}{2\hat{l}_{\text{str}} + \hat{d}_{\text{bead}}} \right)^2} - 1 \right] - \left(\frac{\hat{d}_{\text{bead}}}{\hat{d}_{\text{str}}} \right)^2 \left[\sqrt{1 + \left(\frac{\hat{d}_{\text{str}}}{\hat{d}_{\text{bead}}} \right)^2} - 1 \right] \right\} \quad (\text{B.2})$$

with

$$\hat{\lambda}_{\text{str}} = \frac{2\hat{M}_{\text{str}}}{3\hat{d}_{\text{str}}^2} \quad (\text{B.3})$$

$$\hat{d}_{\text{bead}} = (\hat{N} - \hat{M}_{\text{str}})^{1/3} \quad (\text{B.4})$$

Appendix C. Validity of the Steady-State Approximation

In section 4 we assumed a quasi-static steady-state equilibrium for the beads of the necklace configuration. This approximation is valid if the passage time

$$t_{\text{pass}} = \frac{d_{\text{bead}}}{V} \quad (\text{C.1})$$

is larger than the bead relaxation time t_{rel} .²⁹ To estimate t_{rel} , we consider an infinitesimal deformation of an isolated spherical bead of radius $R = d_{\text{bead}}/2$ into a prolate ellipsoid of major semiaxis $R_> = R + \delta R$ and two identical minor semiaxes $R_< = R - \delta R/2$. This elongated shape ensures that the volume remains constant, $R^3 = R_>R_<^2 + \mathcal{O}(\delta R^2)$. The energy (in units of $k_B T$) of a prolate ellipsoid of eccentricity

$$\epsilon = \sqrt{1 - \left(\frac{R_<}{R_>} \right)^2} \quad (\text{C.2})$$

carrying ϕm_{bead} charged monomers is given by

$$\frac{U}{k_B T} = \frac{3l_B \phi^2 m_{\text{bead}}^2}{5R} (1 - \epsilon^2)^{1/3} \frac{\arctanh \epsilon}{\epsilon} + 2 \left(\frac{R}{\xi_T} \right)^2 (1 - \epsilon^2)^{1/3} \left(1 + \frac{\arcsin \epsilon}{\epsilon \sqrt{1 - \epsilon^2}} \right) \quad (\text{C.3})$$

The first term corresponds to the electrostatic self-energy,^{2,46} while the second term is the surface tension contribution taking the constraint of fixed volume into account.² Performing an expansion about the spherical shape ($\epsilon = 0$) yields

$$\frac{U}{k_B T} = \frac{3l_B \phi^2 m_{\text{bead}}^2}{5R} + 4 \left(\frac{R}{\xi_T} \right)^2 + \left[\frac{8}{5} \left(\frac{R}{\xi_T} \right)^2 - \frac{3l_B \phi^2 m_{\text{bead}}^2}{25R} \right] \left(\frac{\delta R}{R} \right)^2 + \mathcal{O} \left[\left(\frac{\delta R}{R} \right)^3 \right] \quad (\text{C.4})$$

Therefore, keeping only quadratic terms in δR , the relaxation equation reads

$$-6\pi\eta R \frac{dR_{>}}{dt} = \frac{\partial U}{\partial R_{>}} = \frac{2k_B T}{5R^2} \left[8 \left(\frac{R}{\xi_T} \right)^2 - \frac{3l_B \phi^2 m_{\text{bead}}^2}{5R} \right] (R_{>} - R) \quad (\text{C.5})$$

and the ellipsoid relaxes exponentially to the spherical shape with an inverse relaxation time

$$t_{\text{rel}}^{-1} = \frac{2k_B T}{30\pi\eta R^3} \left[8 \left(\frac{R}{\xi_T} \right)^2 - \frac{3l_B \phi^2 m_{\text{bead}}^2}{5R} \right] \quad (\text{C.6})$$

For the range of parameters corresponding to Figure 10, the ratio between the passage and the relaxation times,

$$\frac{t_{\text{pass}}}{t_{\text{rel}}} = \frac{16k_B T}{15\pi\eta V \xi_T^2} \left[1 - \frac{3}{5} \left(\frac{d_{\text{bead}}}{D} \right)^3 \right] \quad (\text{C.7})$$

is always larger than one, and therefore a quasi-static approximation is allowed.

References and Notes

- (1) Barrat, J.-L.; Joanny, J.-F. *Adv. Chem. Phys.* **1996**, *94*, 1.
- (2) Kantor, Y.; Kardar, M. *Europhys. Lett.* **1994**, *27*, 643; *Phys. Rev. E* **1995**, *51*, 1299.
- (3) Dobrynin, A. V.; Rubinstein, M.; Obukhov, S. P. *Macromolecules* **1996**, *29*, 2974.
- (4) Solis, F. J.; Olvera de la Cruz, M. *Macromolecules* **1998**, *31*, 5502.
- (5) Lyulin, A. V.; Dünweg, B.; Borisov, O. V.; Darinskii, A. A. *Macromolecules* **1999**, *32*, 3264.
- (6) Essafi, W.; Lafuma, F.; Williams, C. E. *J. Phys. II* **1995**, *5*, 1269.
- (7) Dobrynin, A. V.; Rubinstein, M. *Macromolecules* **1999**, *32*, 915.
- (8) Lee, N.; Thirumalai, D. Preprint cond-mat/9907199.
- (9) Khokhlov, A. R. *J. Phys. A* **1980**, *13*, 979.
- (10) Schiessel, H.; Pincus, P. *Macromolecules* **1998**, *31*, 7953.
- (11) Schiessel, H. *Macromolecules* **1999**, *32*, 5673.
- (12) Micka, U.; Holm, C.; Kremer, K. *Langmuir* **1999**, *15*, 4033.
- (13) Micka, U.; Kremer, K. *Europhys. Lett.* **2000**, *49*, 189.
- (14) Mehta, A. D.; Rief, M.; Spudich, J. A.; Smith, D. A.; Simmons, R. M. *Science* **1999**, *283*, 1689.
- (15) Perkins, T. T.; Quake, S. R.; Smith, D. E.; Chu, S. *Science* **1994**, *264*, 822.
- (16) Perkins, T. T.; Smith, D. E.; Larson, R. G.; Chu, S. *Science* **1995**, *268*, 83.
- (17) Smith, S. B.; Cui, Y.; Bustamante, C. *Science* **1996**, *271*, 795.
- (18) Perkins, T. T.; Smith, D. E.; Chu, S. *Science* **1997**, *276*, 2016.
- (19) Cui, Y.; Bustamante, C. *Proc. Natl. Acad. Sci. U.S.A.* **2000**, *97*, 127.
- (20) Rief, M.; Oesterhelt, F.; Heymann, B.; Gaub, H. E. *Science* **1997**, *275*, 1295.
- (21) Erickson, H. P. *Science* **1997**, *276*, 1090.
- (22) Tskhovrebova, L.; Trinick, J.; Sleep, J. A.; Simmons, R. M. *Nature* **1997**, *387*, 308.
- (23) Kellermayer, M. S. Z.; Smith, S. B.; Granzier, H. L.; Bustamante, C. *Science* **1997**, *276*, 1112.
- (24) Rief, M.; Gautel, M.; Oesterhelt, F.; Fernandez, J. M.; Gaub, H. E. *Science* **1997**, *276*, 1109.
- (25) Viani, M. B.; Schäffer, T. E.; Paloczi, G. T.; Pietrasanta, L. I.; Smith, B. L.; Thompson, J. B.; Richter, M.; Rief, M.; Gaub, H. E.; Plaxco, K. W.; Cleland, A. N.; Hansma, H. G.; Hansma, P. K. *Rev. Sci. Instrum.* **1999**, *70*, 4300.
- (26) Rief, M.; Fernandez, J. M.; Gaub, H. E. *Phys. Rev. Lett.* **1998**, *81*, 4764.
- (27) Ahsan, A.; Rudnick, J.; Bruinsma, R. *Biophys. J.* **1998**, *74*, 132.
- (28) Halperin, A.; Zhulina, E. B. *Europhys. Lett.* **1991**, *15*, 417.
- (29) Buguin, A.; Brochard-Wyart, F. *Macromolecules* **1996**, *29*, 4937.
- (30) Lee, N.; Thirumalai, D. *Eur. Phys. J. B* **1999**, *12*, 599.
- (31) Tamashiro, M. N.; Schiessel, H. Preprint.
- (32) de Gennes, P.-G. *Scaling Concepts in Polymer Physics*; Cornell University Press: Ithaca, NY, 1985.
- (33) Lifshitz, I. M.; Grosberg, A. Y.; Khokhlov, A. R. *Rev. Mod. Phys.* **1978**, *50*, 683.
- (34) de Gennes, P.-G.; Pincus, P.; Velasco, R. M.; Brochard, F. *J. Phys. (Paris)* **1976**, *37*, 1461.
- (35) Pincus, P. *Macromolecules* **1976**, *9*, 386.
- (36) Rayleigh, Lord. *Philos. Mag.* **1882**, *14*, 184.
- (37) Châtellier, X.; Senden, T. J.; Joanny, J.-F.; di Meglio, J.-M. *Europhys. Lett.* **1998**, *41*, 303.
- (38) Châtellier, X.; Joanny, J.-F. *Phys. Rev. E* **1998**, *57*, 6923.
- (39) Titantah, J. T.; Pierleoni, C.; Ryckaert, J.-P. *Phys. Rev. E* **1999**, *60*, 7010.
- (40) Borisov, O. V.; Halperin, A. *Eur. Phys. J. B* **1999**, *9*, 251 and references therein.
- (41) Schiessel, H.; Bruinsma, R.; Gelbart, W. M. Preprint.
- (42) van Holde, K. E. In *Chromatin*; Rich, A., Ed.; Springer-Verlag: New York, 1988.
- (43) Klimov, D. K.; Thirumalai, D. *Proc. Natl. Acad. Sci. U.S.A.* **1999**, *96*, 6166.
- (44) Soddemann, T.; Schiessel, H.; Blumen, A. *Phys. Rev. E* **1998**, *57*, 2081 and references therein.
- (45) Vilgis, T. A.; Johner, A.; Joanny, J.-F. Preprint cond-mat/0001140, to appear in *Eur. Phys. J. E*.
- (46) Wendt, G. In *Handbuch der Physik*; Flügge, S., Ed.; Springer-Verlag: Berlin, 1958; Vol. 16.
- (47) Gradshteyn, I. S.; Ryzhik, I. M. *Table of Integrals, Series, and Products*, 5th ed.; Jeffrey, A., Ed.; Academic Press: San Diego, 1994.

MA992025S